archives
of thermodynamics
Vol. **44**(2023), No. 4, 665–704
DOI: 10.24425/ather.2023.149737

Overview of application options for vertical axis wind turbines

WALDEMAR KUCZYŃSKI[a*]
IWONA MICHALSKA-POŻOGA[b]
MARCIN SZCZEPANEK[c]
KRZYSZTOF CHMIEL

[a] Technical University of Koszalin, Faculty of Mechanical Engineering and Energy, Department of Energy, Racławicka 15-17, 75-620 Koszalin, Poland

[b] Technical University of Koszalin, Faculty of Mechanical Engineering and Energy, Department of Food Processes and Equipment, Racławicka 15-17, 75-620 Koszalin, Poland

[c] Maritime University of Technology of Szczecin, Faculty of Mechanical Engineering, Willowa 2, 75-500 Szczecin, Poland

Abstract The article presents an analysis of the use of Savonius wind turbines with vertical axis of rotation. The first part presents an analysis of the literature with the dentification of the properties of the basic atmospheric parameters related to the air movement referred to as wind. Used mathematical descriptions used in the analysis of air movement and enabling the identification of basic thermodynamic parameters of wind turbines with a vertical axis of rotation were presented. Then, the historical background of the development of wind turbines with a vertical axis of rotation was presented, and constructions of this type currently used were described. Proposals for modification of the configuration and design of Savonius rotors and the impact of these activities on their efficiency were analyzed. These issues were presented in relation to the experimental work carried out in the international research centers. Obvious advantages and disadvantages of using this type of equipment in the field of wind energy were indicated.

Keywords: Wind energy; Wind turbines; Savonius' law

*Corresponding Author. Email: waldemar.kuczynski@tu.koszalin.pl

Nomenclature

C_D	–	drag coefficient
c_p	–	Betz coefficient
P	–	mechanical power, W
Re	–	Reynolds number
T, t	–	temperature, K, °C, respectively
VAWT	–	vertical axis wind turbine
$\mathbf{v}$	–	air speed, m/s

Greek symbols

μ	–	dynamic viscosity, Pa·s
ν	–	kinematic viscosity, m^2/s
ρ	–	density, kg/m^3
λ	–	speed factor (ratio)

1 Introduction

The constantly growing demand for energy in recent decades has created global concerns about the consequences of the massive exploitation of non-renewable energy sources such as pollution, global warming and the reduction of the political and economic profitability of using non-renewable energy resources. This forced the search for alternative and renewable energy sources.

Wind energy is a serious competitor among renewable resources and it also complements other energy sources. It is one of the most promising sources of renewable energy: pollution-free, widely available in the Earth's atmosphere, and locally transformable thus it may help reduce dependence on fossil fuels. Many developed and developing countries have realized the importance of wind as an important resource for energy production, and all over the world the necessary measures are being taken to use this energy for its efficient use in energy production.

Electricity storage and distribution is still a serious problem, especially when the amount produced varies considerably over time and place, such as in the case of wind energy. A compact, low-speed vertical axis wind turbine (VAWT) machine such as the Savonius turbine seems to be particularly promising as it can be used for local electricity production in urban, rural and less accessible areas, as well as for collecting climate data. The use of unconventional devices such as the Savonius wind turbine is a low cost solution with a lower environmental impact for decentralized power generation. VAWT concepts are suitable for generating electricity in conditions

where traditional designs, such as high wind speeds and turbulent flows are not applicable. Savonius turbines have been proposed as an alternative to distributed energy and are the focus of the recent research.

2 The air in the Earth's atmosphere

Atmospheric air in the ground layer is an approximately homogeneous mixture of gases, including: nitrogen 78.09%, oxygen 20.95%, argon 0.93%, carbon dioxide 0.03% and neon, helium, krypton, xenon, hydrogen and ozone up to 0.003% in total. Moreover, the air consists of water vapor, dust pollutants and gases of volcanic, organic and industrial origin. The content of the air composition does not change up to the height of about 80 km, i.e. Mesopause, as shown in Fig. 1, where the vertical distribution of the mean temperature of the atmosphere is presented [1].

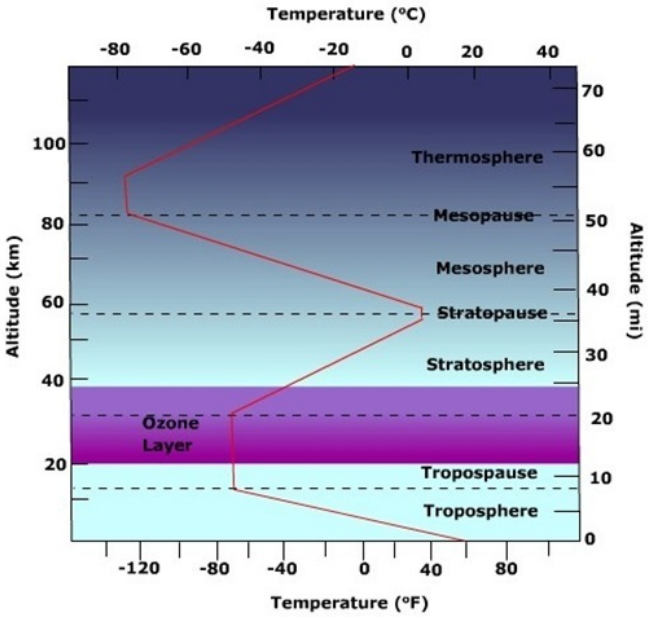

Figure 1: Diagram of the Earth atmosphere into layers [2].

On the other hand, considerations in the field of wind energy concern the troposphere, because it contains about 80% of the total air mass and almost all water vapor in the Earth's atmosphere. It identifies the so-called normal conditions adopted in meteorology and wind energy as average values:

- air temperature $t = 15°\text{C}$ (288 K),
- air pressure $p = 1013$ hPa,
- air volume density $\rho = 1.255$ kg/m^3,
- dynamic viscosity $\mu = 1.7894 \cdot 10^{-5}$ Pa·s,
- kinematic viscosity $\nu = \mu/p = 1.4607 \cdot 10^{-5}$ m^2/s.

According to an approximate formula, the dynamic viscosity of the air μ in the low pressure range does not depend on the air density ρ or the atmospheric pressure p, but on the temperature T:

$$\mu = \mu_0 \left(\frac{T}{T_0}\right)^{0.76}, \tag{1}$$

where $T_0 = 273$ K, $\mu_0 = 1.71 \cdot 10^{-5}$ Pa·s.

As the altitude increases, the air pressure, temperature and density change (Fig. 2, where H is the height and τ temperature). The dependence of temperature on altitude is not uniform in different latitudes, its value can be identified, for example, from the correlation shown in Fig. 3.

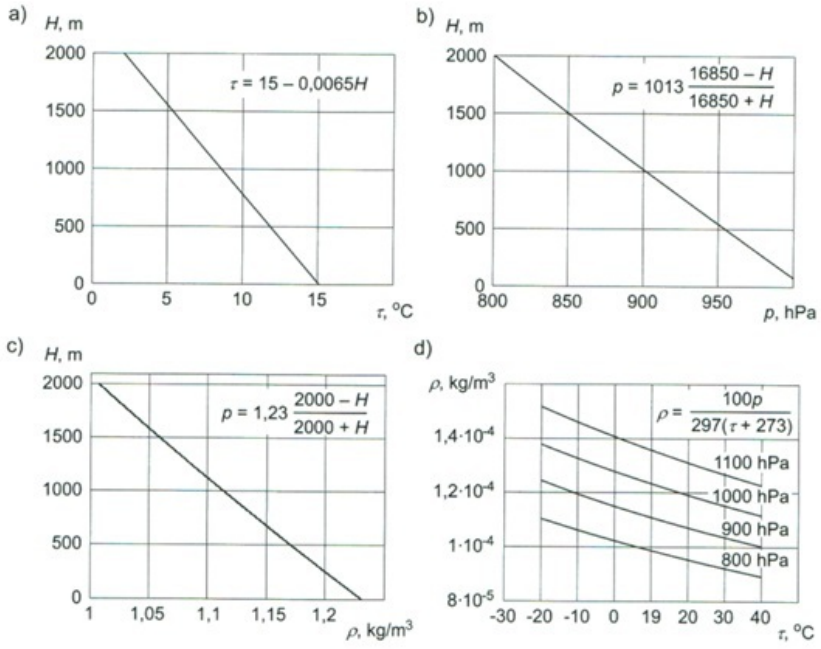

Figure 2: Characteristics of the dry air [1].

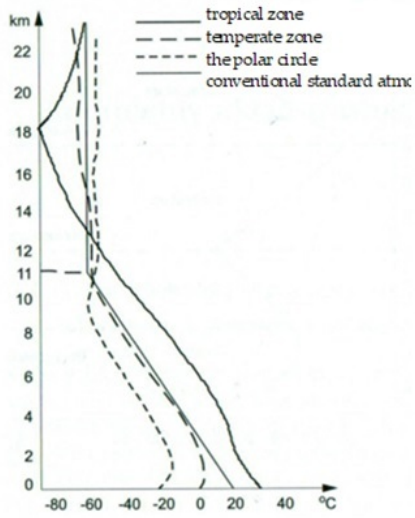

Figure 3: Temperature dependence on altitude in different latitudes [1].

The average values up to a height of 11 km are determined from the following formulas:

$$t = t_0 - 0.0065H\,, \tag{2}$$

$$t = t_{\text{real}} - 0.0065H\,, \tag{3}$$

$$\rho = \rho_0 \frac{20000 - H}{20000 + H}\,, \tag{4}$$

where t_0 is 15°C, t_{real} – actual temperature at the place of measurement, ρ_0 – air density.

2.1 The movement of air masses

The air in the Earth's atmosphere is in constant motion relative to the Earth's surface. This phenomenon is called wind. The main reason for the formation of wind is the incidence of electromagnetic radiation of the Sun on the Earth's surface, which causes its uneven heating and the formation of a pressure difference. The movement of air masses takes place from high to low pressure and is the more intense the greater the pressure difference and depends on the distance of media with different pressures as well as on the terrain.

The movement of air masses in the Earth's atmosphere is a very complex phenomenon. Heating of air in the equatorial zone causes air masses to move vertically and then splits into two streams in the upper atmosphere towards the north and south poles and in the opposite direction in the ground layer (Fig. 4). The direction of the wind depends on the centrifugal forces caused by the rotation of the Earth and the Coriolis force [1,3].

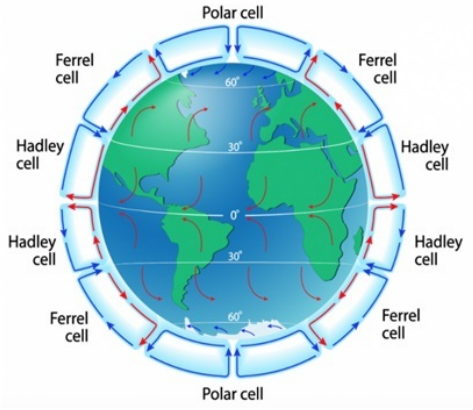

Figure 4: Diagram of the circulation of the Earth's atmosphere [4].

The direction and speed of the wind change throughout the day. This phenomenon results from the faster heating and cooling of the land surface than the surface of water reservoirs. The result is the daytime sea breeze, i.e. the wind blowing from the sea towards the land. The opposite phenomenon occurs at night, when water gives off heat more slowly than land, when the pressure above the surface of the water is lower than the pressure above the surface of the land. The night land breeze takes the opposite direction to the day one and brings dry air with it above the water surface [5]. Another important phenomenon is the faster heating and cooling of mountain slopes from the valleys. The slopes on the southern side heat up intensively, at the same time heating the air in contact with the surface of the slopes, after which it expands and rises upwards on the slopes creating a daily valley slope wind. Sometimes this type of wind causes the formation of clouds on mountain peaks. The opposite occurs at night, when the air adjacent to the slopes cools down more than the air at the same height above the valley. The more cooled air is heavier, so it falls down the slopes, causing mountain slope winds [5]. Wind machines using this phenomenon, i.e. moving in the direction of the air mass flow and using head pressure, are presented below.

2.2 Characteristics of wind machines

When the wind acts on solids, it encounters resistance, while the bodies, under the influence of the wind, are subjected to forces called pressure. A necessary condition for keeping the body at rest is the application of a force equal to the pushing force, but directed in the opposite direction. Relative air velocity in relation to the body is important, but it is irrelevant whether the body moves in relation to the stationary air or vice versa, i.e. air in relation to the stationary body. The wind action related to the area of the largest cross-section of the body perpendicular to the wind direction is called the frontal drag coefficient. Thus, the force exerted by the wind on the bodies at rest is the force against the frontal resistance which the body encounters as it moves in still air.

One of the simplest types of wind machines is the one that moves along a straight line under the influence of the wind. The drag device can be considered with a model of a trolley propelled by a collinear wind with velocity v pushing against the transverse surface A, and the condition must be $v > u$ [6].

Based on [7], the force driving the engine using the frontal wind pressure of speed v acting on the plane of the rotor blades with surface A in accordance with the lifting speed u is

$$P = \frac{1}{2}\rho C_D A(v-u)^2 = \frac{1}{2}\rho C_D A\left(v^2 - 2uv + u^2\right). \tag{5}$$

The concave side of the rotor blades rotates in line with the thrust force driving the rotor, while the convex side turns in the opposite direction, so the resultant of the forces is the difference of these forces:

$$\begin{aligned} P &= \frac{1}{2}\rho C_{D_1} A(v-u)^2 - \frac{1}{2}\rho C_{D_2} A(v+u)^2 \\ &= \frac{1}{2}\rho A\left[C_{D_1}(v-u)^2 - C_{D_2}(v+u)^2\right]. \end{aligned} \tag{6}$$

Disregarding the frictional forces and in the absence of load on the wind turbine, this force is

$$P = \frac{1}{2}\rho A\left[C_{D_1}(v-u)^2 - C_{D_2}(v+u)^2\right] = 0. \tag{7}$$

The wind speed relative to the carriage is (vu) while C_D is the drag coefficient. An analogy of the turbine speed discriminant is the dimensionless

carriage speed defined as λ, which is

$$\lambda = \frac{u}{v}\,, \tag{8}$$

then

$$P = \frac{1}{2}\rho C_D A v^2 \left(1 - 2\lambda + \lambda^2\right). \tag{9}$$

The product of the driving force and the speed of the carriage defines the power obtained from the flow:

$$P = Tu = \frac{1}{2}\rho C_D A v^3 \lambda \left(1 - 2\lambda + \lambda^2\right). \tag{10}$$

The c_p power factor is

$$c_p = \frac{P}{\frac{1}{2}\rho v^3 A} = \frac{\frac{1}{2}\rho C_D A v^3 \lambda \left(1 - 2\lambda + \lambda^2\right)}{\frac{1}{2}\rho v^3 A} = \lambda \left(1 - 2\lambda + \lambda^2\right) C_D\,. \tag{11}$$

The power factor c_p reaches its maximum if

$$\frac{dc_p}{d\lambda} = 0, \tag{12}$$

so

$$\lambda|_{c_{p\max}} = \frac{1}{3} \tag{13}$$

and

$$c_{p_{\max}} = \frac{4}{27} C_D = 0.148 C_D\,. \tag{14}$$

The maximum drag coefficient for a concave hemispherical surface subjected to frontal wind pressure (according [7]) is $C_D = 1.33$. The maximum power factor for a turbine using a concave surface perpendicular to the direction of wind flow is

$$c_{p_{\max}} = 0.148 C_D = 0.148 \cdot 1.33 = 0.197. \tag{15}$$

This means that the theoretical maximum use of wind energy in a device using frontal pressure is about 20% of the energy of the raw wind stream.

2.3 Savonius turbine mathematical model

The mathematical model based on the pressure drop on both sides of a rotor with a vertical axis of rotation was first proposed by Chauvin and Benghrib [8] to determine the power of a classic Savonius two-bladed turbine (Fig. 5).

If $\vec{\omega} = \dot{\alpha}\vec{k}$ is a vector of instantaneous rotation and due to the symmetry of the Savonius rotor $\dot{\alpha} = \vec{\omega} = \text{const}$ then the torque Q is equal to

$$Q = \sum_i \left(\overrightarrow{OM} \times \vec{F}_i\right) \cdot \vec{k}. \tag{16}$$

The above sum has two components:

$$Q = Q_M + Q_D\,, \tag{17}$$

where: Q_M – pressure component, Q_D – drag component.

Assuming that the pressure difference on the braked blade and the driven blade is Δp_M and Δp_D, respectively, the total driving torque can be written as

$$Q = 2r^2 H \int_0^{\pi/2} (\Delta p_M - \Delta p_D) \sin 2\theta \, d\theta. \tag{18}$$

The mean power P obtained by integrating the torque from 0 to π:

$$P = \omega Q = \frac{\omega}{\pi} \int_0^{\pi} Q \, d\alpha. \tag{19}$$

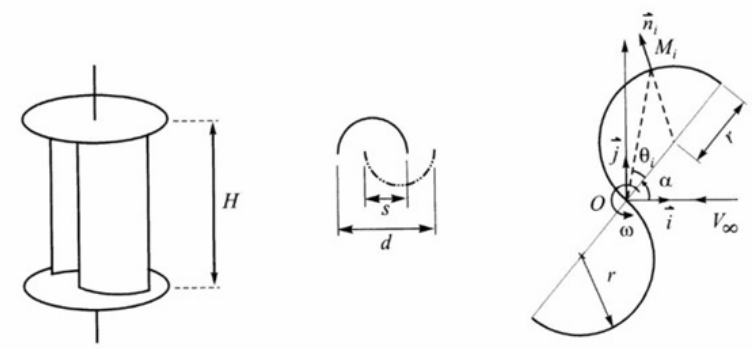

Figure 5: Savonius rotor-calculation diagram [9].

Whereas the power factor c_p is

$$c_p^* = \frac{P}{\frac{1}{2}\rho V^3 (4rH)}, \tag{20}$$

where r is the radius of the Savonius rotor with the aperture ratio $s/d = 0$ (r, s and d, see Fig. 5). In this case, the face of the turbine is the same as the total area washed by the turbine. After carrying out the experiments, Chauvin [8] proposed the pressure distribution according to the formula

$$\frac{\Delta p_M^{(i)}}{\frac{1}{2}\rho V_e^2} = K, \tag{21}$$

where K is a sinusoidal function α (α, see Fig. 5).

The total flow velocity $\vec{V}_e$ is the difference between the undisturbed flow velocity $\vec{V}_\infty$ and the absolute velocity of the point M_i of the rotor blade $\vec{V}_i$:

$$\vec{V}_e = \vec{V}_\infty - \vec{V}_i\,. \tag{22}$$

The component Q_M of the torque is

$$Q_M = \rho r^2 H K \left(V_\infty^2 + 2\dot{\alpha}^2 r^2 - \frac{\pi}{2} V_\infty \dot{\alpha} r \cos\alpha - 2 V_\infty \dot{\alpha} r \sin\alpha \right). \tag{23}$$

The pressure distribution was assumed to calculate the torque Q_D component (Eq. (25)):

$$\frac{\Delta p_D^{(i)}}{\frac{1}{2}\rho V_i^2} = K'\,, \tag{24}$$

so

$$Q_D = 2\rho r^4 H \dot{\alpha}^2 K'. \tag{25}$$

The pressure difference on both sides of the turbine blade at seven points k of the blade is shown in Fig. 6 for both driving and braking half-cycles [9].

The experimental starting torque for a full revolution of the turbine is shown in Fig. 7, which shows that the braking component is negligibly small compared to the driving component.

Using Eqs. (11)–(17) the approximate value of the power factor c_p^* was determined, which is a function of the speed ratio:

$$c_p^* = \frac{K\lambda}{2}\frac{1}{2} - \frac{K\lambda^2}{2\pi} + \frac{K - K'}{K}\frac{\lambda^3}{4}\,. \tag{26}$$

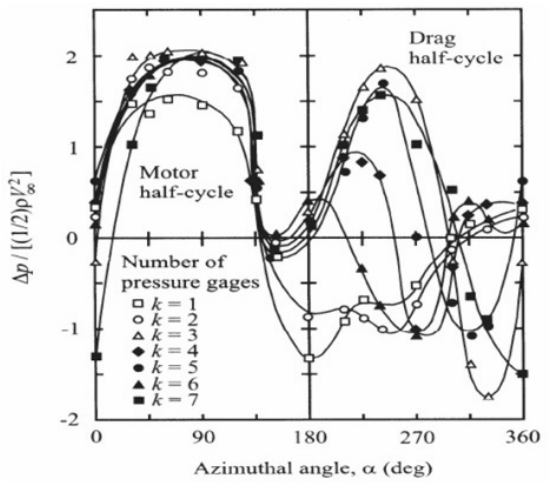

Figure 6: Pressure distribution as a function of the azimuthal angle [9].

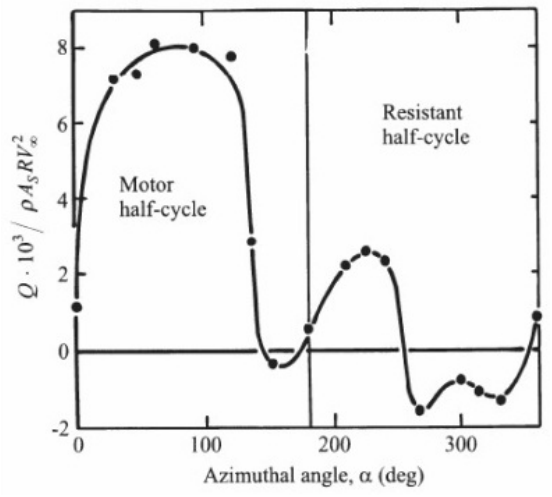

Figure 7: Starting torque when starting the turbine [9].

This equation in graphic form is a family of curves dependent on the parameter K'. Physically, a solution exists for $K' \geq 0.73K$. If we take $K' = K$, we can omit the term containing λ^3 which has no physical dimension. Then

$$c_p^* = K\frac{\lambda}{2}\left[\frac{1}{2} - \frac{\lambda}{\pi}\right] = c_{p_m}^* 16\left(\frac{\lambda}{\pi}\right)\left[\frac{1}{2} - \left(\frac{\lambda}{\pi}\right)\right], \tag{27}$$

where $c_{p_m}^* = 0.17$ for $\lambda_M = 0.78$.

The limiting value of the speed-specific discriminant is $\lambda L = 2\lambda_M = 1.57$. The normalized power factor was compared with the experimental data of other researchers. The differences between the mathematical and experimental model are the result of not taking into account the frictional forces and the fact that the experimental model had a gap with the parameters $s/d = 0.25$. Figure 8 shows the results of tests by Chauvin and other researchers, on the basis of which the maximum value of the power factor was determined to be approximately 0.17 [8].

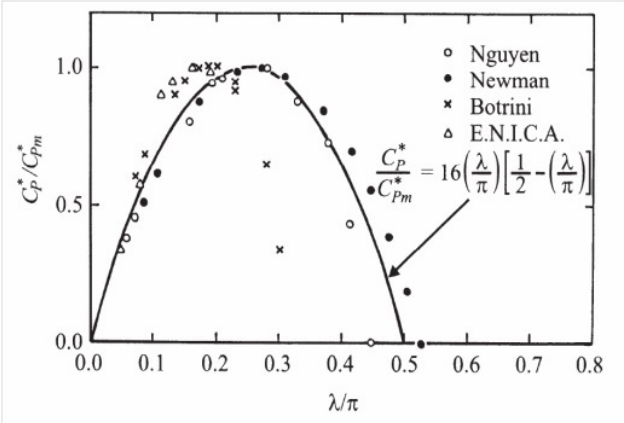

Figure 8: Power factor as a function of the speed index [8].

3 Wind turbines – historical background

The first devices using headwind pressure were used more than 3000 years ago. The use of a turbine with a vertical axis of rotation made it possible to connect the drive shaft directly to the rotor to a mechanical load at ground level and was used for grinding grain and pumping water. The earliest records of the use of wind energy come from the East [10–14]. Some concepts of a windmill-like device described in Pneumatica, probably in the first century AD: a Dutch rotor driving a disk with four pins that repeatedly raise the piston in an air pump [15] – Fig. 9a, a device with a rotor water mill [16] – Figs. 9b and 9c, sketch of Heron's drive according to Alexandria and Schmidt [16] – Fig. 9c. According to Drachmann [14], Fig. 9c shows the closest to the original interpretation of the sketch of a primitive Heron drive based on a wind rotor. It was concluded that the device shown in Fig. 9 may have been a toy and not a working use-full machine.

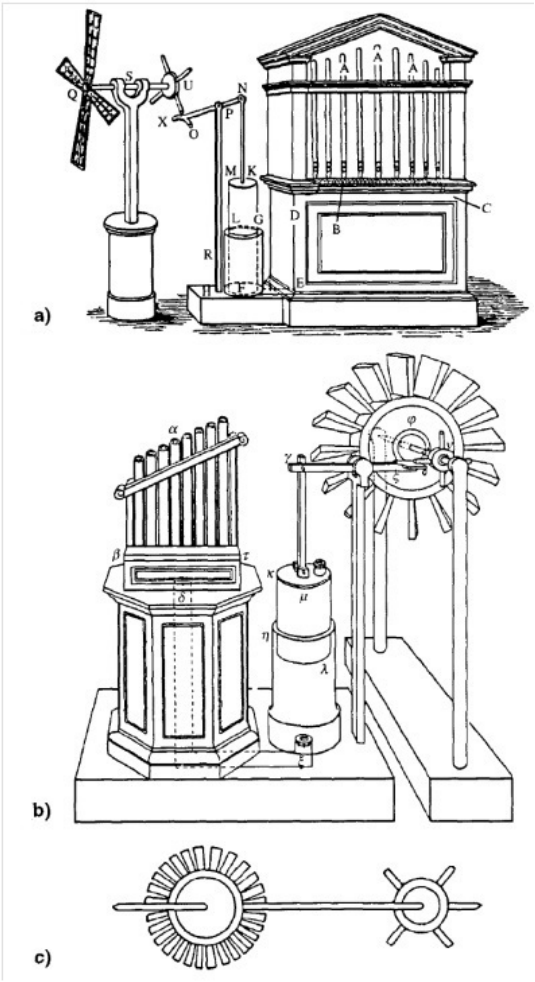

Figure 9: Some concepts of a windmill-like device described by Heron of Alexandria in Pneumatica [16]: a) a Dutch rotor driving a disc with four pins, b) a device with a water-mill rotor, c) sketch of Heron's drive.

The second construction was a Persian windmill with a vertical axis of rotation. Al-most all the notes from the period of 1st−12th century AD come from the Middle East and Central Asia, which is why these regions of the world were considered the cradle of the windmill. The first documented use of a windmill dates back to the 10th century AD from Persia. The records and reliable drawings correspond to the remains of ancient and modern mills, which are still in use today [17, 18].

Around 1300, the Syrian cosmographer al-Dimashqi (1256–1326) provided a detailed description and drawing of a two-story walled structure with millstones on top and a rotor on the bottom consisting of a spoked reel with vertical ribs covered with fabric, forming the sails. The wall surrounding the structure was equipped with slots corresponding to the height of the rotor, and in the upper part of the wall, the circumference towards the center (above the rotor) was reduced to achieve a higher wind speed in the rotor, regardless of the direction.

In 1963, Wulff [19] observed about 50 windmills of still in operation Neh. The structure consisted of a rotor about 5.5 m high and 4.3 m in diameter closed in the side walls about 6.5 m high and a half-wall which leaves a 2.2 m wide opening facing north, the main wind direction. The central wooden shaft was about 0.43 m in diameter. The lower end extending down the mill chamber contained a steel pinch which rested on a wooden pinch block in a chamber lined with a lubricating backing consisting of multiple layers of cloth soaked in tallow. The upper millstone was attached to a steel mandrel, and the lower stone, 2 m in diameter, rested on a brick structure. Eight blades are attached directly to the rotor shaft, while the rotor blades are made of several long bundles of reeds pressed with tie rods, approximately 0.56 m wide and 0.15 m thick. The tie bars are attached with pegs and ropes to several sets of guy ropes that tie together the rotor assembly (Fig. 10).

The joint system was insufficiently stiff to operate stably and the thrust block with a tallow soaked grease pad acting as a bearing was imprecise, which required the system to be adjusted frequently in order for the millstones to function with sufficient clearance.

Wulff [19] gives several figures relating to the performance of these mills. When he visited Neh in 1963, there were 50 more mills, each milling an average of 1 ton of grain in 24 hours, so a total of 6000 tons of flour were produced during the 120-day wind season. Based on a wind speed of about 30 m/s, effective turbine exposure to 1.5 rotor blades, and a mill efficiency of 50%, Wulff estimated the output power to be about 75 hp per mill. The calculations were overestimated as the power calculation with the same assumptions is based on the aerodynamic drag according to the equation

$$c_p = \frac{P}{\frac{1}{2}\rho v^3 A}\,, \tag{28}$$

which would allow to obtain a maximum of 22 hp at a wind speed of 30 m/s.

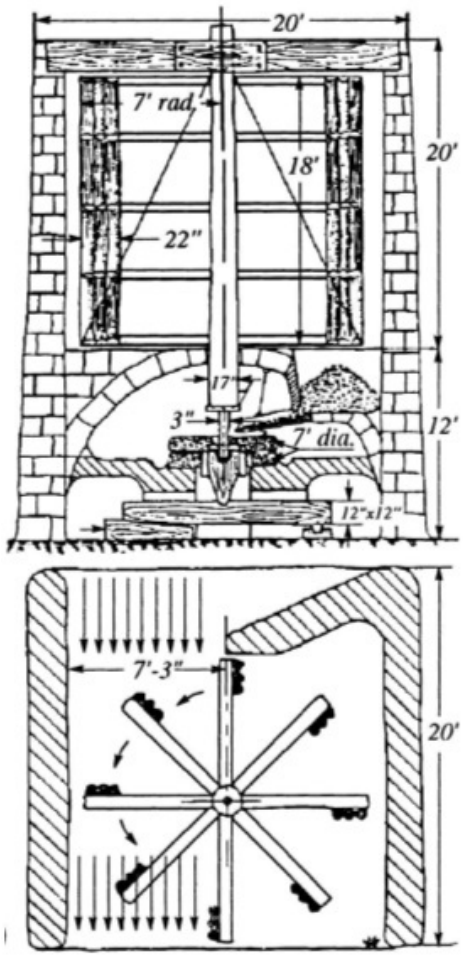

Figure 10: Existing Persian-type windmill in Neh (sketch of the construction and operation of the windmill) [19].

Wulff [19] suggests that the earlier concept was taken from an ancient Norse or Greek water mill, in which the mill itself had to be placed above the water wheel. Relocating the rotor improved efficiency by exposing the rotor to higher wind speeds and certainly made handling much easier. Other noticeable changes are the use of reed instead of cloth as the work surface and the use of a single wind gap instead of the four described by al-Dimashqi, although this may have been limited to the region around the Neh, where the wind blows steadily from the north in summer.

It is commonly claimed that the windmill was invented in China more than 2000 years ago, but Needham [11] states that the earliest record dates from 1219. Chinese mills have a characteristic form with eight sails mounted on masts around a vertical axis, arranged in a way that allows their automatic alignment. Figure 11a shows the arrangement of masts supported on the rotor shaft by radial crossbars. The power is taken off by means of a rectangular drive consisting of toothed wheels with pin teeth. Figure 11b illustrates the operation of the sails during the rotation of the rotor. Each sail was mounted asymmetrically and held against the wind by a rope (positions G, H, A, and B) until it reached a pivot point where it pivots, flips and leans outwards (C and D), from there entering the wind axis skew, which resulted in the generation of low shaft rotation resistance forces (E and F). Thanks to this solution, curtain walls such as in Sistan were not used and wind from any direction was used.

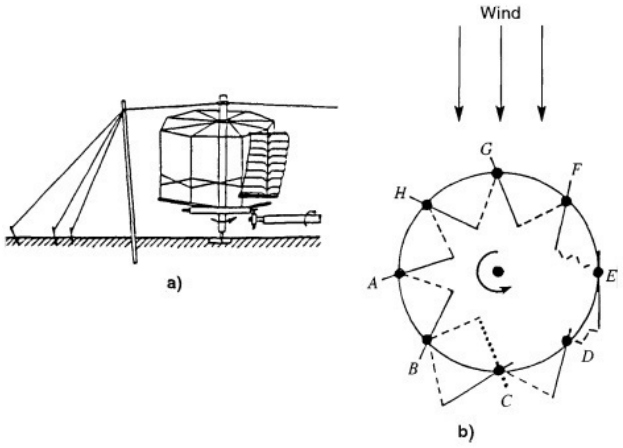

Figure 11: Chinese windmill with a vertical axis of rotation [20]: a) general arrangement of sails, masts, main shaft and power take-off, b) automatic positioning of the sails during rotation; in positions E and F the sails deflect with little resistance.

This type of mill is still used in eastern China. The Chinese vertical windmill construction, unlike the Persian one, was used in north-western Europe. At the end of the 12th century, the concept of windmills with a horizontal axis of rotation was created. Over the next years, windmills of this type were improved and used throughout Europe, but the prototype of this solution was the device described by Heron

4 Modern turbines with a vertical axis of rotation

4.1 Types of turbines with a vertical axis of rotation and their characteristics

Units with a vertical axis of rotation can be divided into two types: the first, where the working blades move slower than the wind, and the second, where the blades move faster than the wind (Fig. 12).

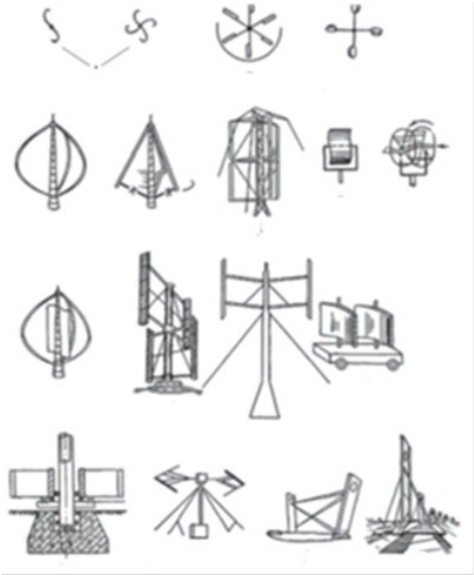

Figure 12: Various rotor designs with vertical axis of rotation [21].

Units of the first type (Fig. 12), are characterized by a low wind power utilization factor (less than 0.3), low rotational speed (the optimal blade speed is about 0.3–0.7 wind speed), which requires the use of heavy mechanical and electrical equipment to obtain electricity.

The high velocity orthogonal units (Fig. 12, items 8–18) convert the work done by the forces arising from the outflow of the rotor blade profile with aerodynamic profiles with a smoothly shaped leading edge. An important advantage of machines with a vertical spin axis is their independence from the wind direction.

Front wind pressure devices were not improved from the early Middle Ages to the beginning of the 20th century. Concepts similar to modern ones

were built and tested intensively in the years 1920–1930 and found a new application with the invention of a new type of rotor: the Savonius turbine and the Darrieus turbine.

The Savonius turbine was invented by the Finnish engineer S.J. Savonius in 1922. The straight Savonius rotor is S-shaped in cross section, which can be made by cutting the barrel in half, inverting one of the halves and joining them together (Fig. 5).

The original Savonius rotor models were able to achieve a maximum efficiency of less than 20%. The dependencies of the power factor and torque on the speed factor of various designs of wind turbines are shown in Figs. 13 and 14.

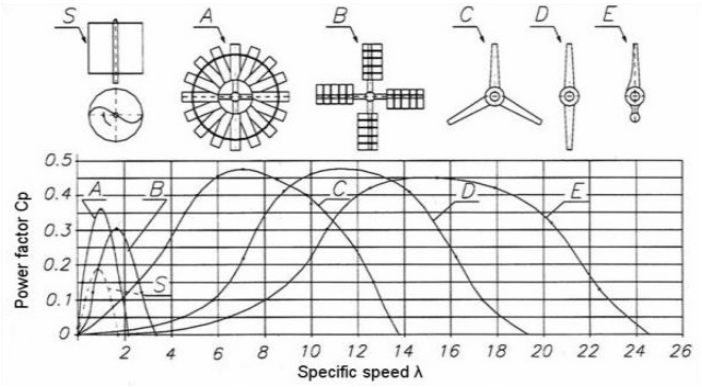

Figure 13: Dependence of the wind energy utilization coefficient C_p on the speed factor λ and the number of blades of the rotor and Savonius rotor [22]: A – multi-blade rotor, B – four-blade rotor, C – three-blade rotor, D – two-blade rotor, E – single-blade rotor, S – Savonius rotor.

A Savonius turbine is only useful and economical for low energy requirements such as pumping water, driving a small electric generator, providing ventilation and mixing water to protect fish ponds in winter conditions, or as an ocean current meter. The technology required to design and manufacture a Savonius rotor is very simple and is recommended for applications in developing countries or in isolated areas without a power grid. The current development and popularization of the Savonius turbine is based on the premise of microgeneration of electric current.

Systematic research carried out by Savonius and later repeated by other scientists under experimental conditions allowed to determine the optimal forms of rotors and to increase the efficiency of advanced structures to the level of 30% (Fig. 15).

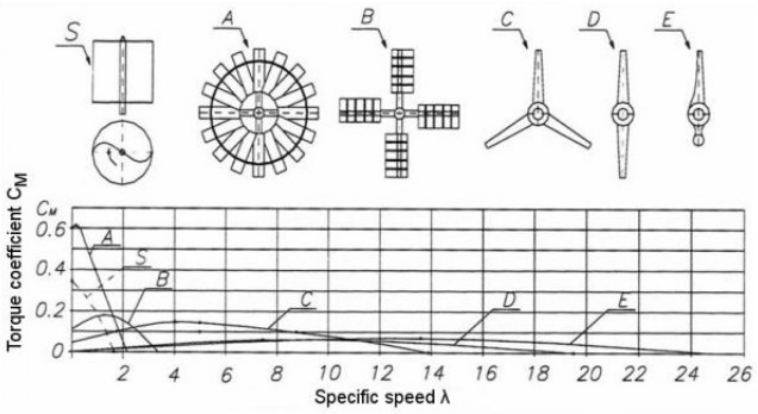

Figure 14: Dependence of the (relative) torque C_M of the function of the high speed discriminant λ and the number of blades of the rotor and the Savonius rotor [22]: A – multi-blade rotor, B – four-blade rotor, C – three-blade rotor, D – two-blade rotor, E – single-blade rotor, S – Savonius rotor.

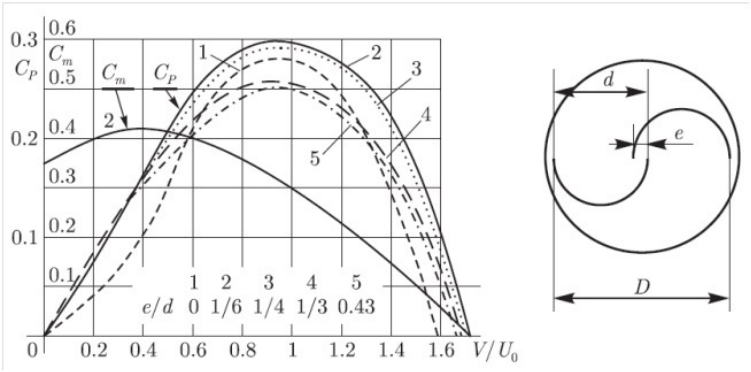

Figure 15: Diagram of dependence of the torque C_m and the power factor C_P of Savonius rotors with different dependencies of the gap between the blades to the diameter of one blade [21].

The efficiency of the system reaches 30% with the thickness of the stream passing from one side of the rotor to the other equal to 1/6 of the diameter of the rotor's working half-cylinder. The efficiency of the rotor increases with the greater relative height and it is not recommended to use a height lower than the rotor diameter.

The Savonius rotor, like many orthogonal machines, has so-called dead zones, i.e. positions in which the rotor will not start to turn on its own,

even though the average torque is quite high (Fig. 15, line C_m). When the rotor is at an angle between 300° and 0°, the pressure coefficient is negative and the rotor will not turn in the required direction (Fig. 16).

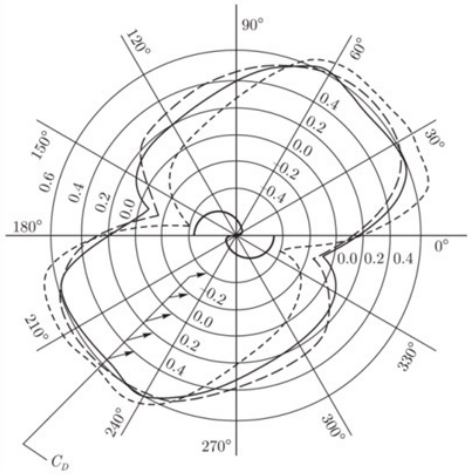

Figure 16: Diagram of the air stream flow through the Savonius turbine with the gap between the blades [21].

This problem was solved by using a multi-level (double) Savonius rotor consisting of two interconnected rotors rotated relative to each other by an angle of 90° (Fig. 17).

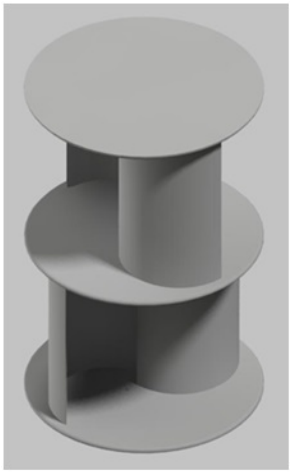

Figure 17: A two-tier Savonius rotor (own elaboration).

4.2 Design improvements to vertical axis wind turbines

Numerous improvements have been made to the low-speed orthogonal units to in-crease energy efficiency. This goal was achieved by introducing control devices that fold the 'sail' at the working element moving in the direction of the wind and unfold the 'sail' at the optimal moment with the working element moving in the direction of the wind (in some inventions this is done automatically, e.g. under the influence of wind force). Due to the low rotational speed, the unit consumption of materials (per unit of power) remains high.

For low-speed machines, the highest possible drag coefficient C_D is required in the place where the working element moves along the flow. The resistance to the working element must be the lowest in the next point of rotation of the turbine. This was achieved by a special form of the rotor blades in the form of moving elements changing their position in relation to the air stream, which allowed to increase the efficiency of VAWT turbines to over 30% (Figs. 18 and 19).

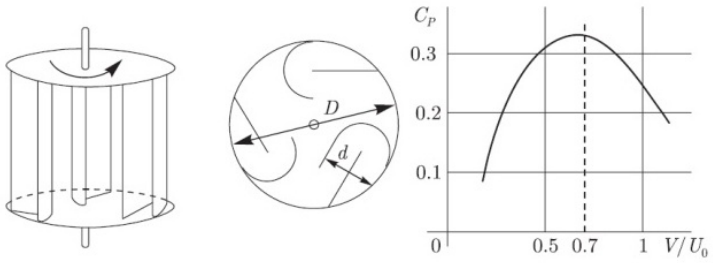

Figure 18: Low-speed rotor with directional fairings [21].

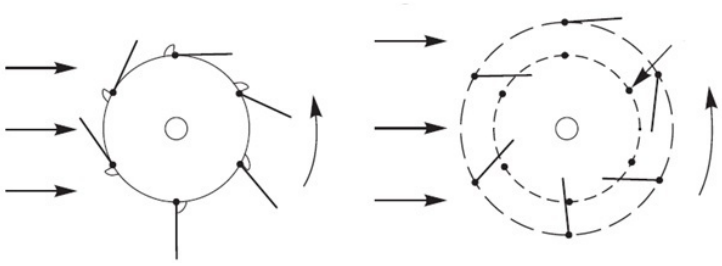

Figure 19: Rotors with rotating plates [21].

Another solution was to equip the blades with an internal flatness on the sides and push them out under the influence of aerodynamic and centrifugal

forces causing the rotor to become almost cylindrical and the blades to move apart in light winds. This solution was implemented in a Lafond turbine with multiple blades (Fig. 20).

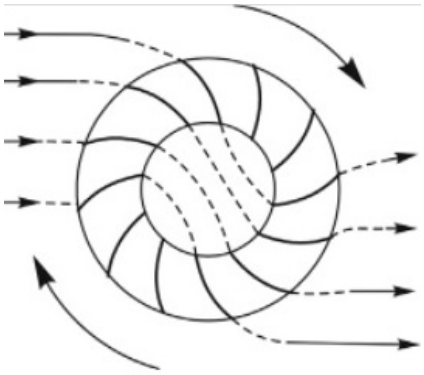

Figure 20: Lafond turbine with many blades [21].

4.3 Influence of Savonius rotor configuration on aerodynamic efficiency

Most significant experimental studies of Savonius rotor configurations were conducted in the 4.9×6.1 m Vought Corporation System Division low-speed wind tunnel commissioned by Sandia Laboratories US Energy Research and Development Administration in 1975. The tests included such parameters such as the number of blades, air stream speed, rotor height and slot width (Table 1).

Table 1: The range of values of various parameters of the Savonius turbine.

Parameters	Unit	Value
Number of rotor's blades	–	2 and 3
Nominal speed of the air stream	m/s	7 and/or 14
Reynolds number per meter	–	$4.32 \cdot 10^5$ and $4.32 \cdot 10^8$
Rotor's height	m	1 and 1.5
Rotor's diameter	m	1
Overlay on containment discs	–	0–0.1
Ratio of the width of the gap between the rotor blades	–	0.0, 0.1, 0.15, 0.20

The measured test variables were torque and rotational speed. The data is presented as power and torque factors as a function of speed (or angular position for static starting torques). It has been determined that increasing the Reynolds number and/or aspect ratio improves efficiency, and the optimal configuration consists of two sets of twin-blade rotors, rotated through 90°, with the slit width being 0.1–0.15 of the width of a single blade.

Representative test models are shown in Figs. 21, 22. The rotor and end disks are made of 6061 T6 aluminum alloy. Each pair of end plates was

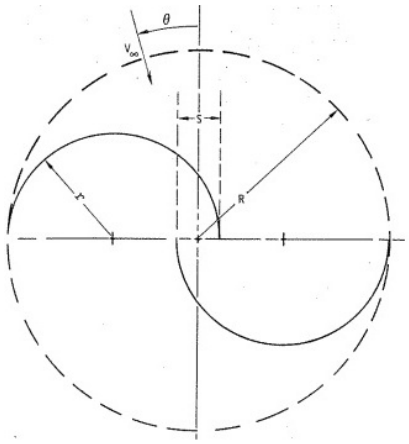

Figure 21: Diagram of a two-blade Savonius rotor shifted by 180° [23].

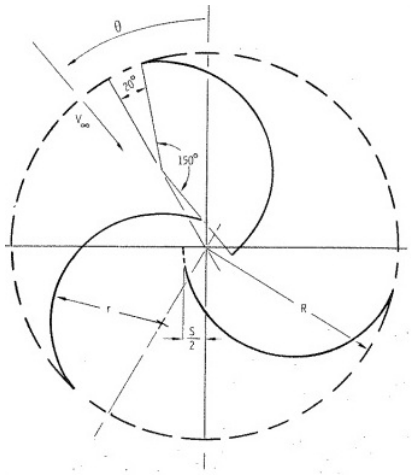

Figure 22: Diagram of a three-blade Savonius rotor with an offset of 150° [23].

adapted to several bucket con-figurations. The rotor was attached to the end plates with machine screws.

The Vought Systems Division Low Speed Wind Tunnel is a closed-circuit facility consisting of 11.9 m rectangular test sections measuring 2.1 m × 3.0 m and 4.6 m × 6.1 m. due to its dimensions and speed range of 3–23 m/s. All instrumentation related to facility handling and wind tunnel flow conditions were provided by Vought. Sandia provided instrumentation related to the measurement of torque and rotational speed of the turbine.

Prior to testing each configuration, the rotor was rotated with an air motor at a very low but constant speed to determine the tare torque due to friction in the bearings. Values of the order of 0.678 J were recorded for each configuration and used to correct the data. A wind tunnel turbulence coefficient of 1.4 was determined, but due to differences between wind speed and rotor speed, the Reynolds number was not corrected.

The object placed in the wind tunnel causes the creation of a tunnel blockade, which causes an increase in the local wind speed on the test section. This increase was taken into account by determining the tunnel congestion coefficient ξ called the speed increase. The total factor is the sum of the speed gain due to excitation lock and permanent lock. It is very difficult to pinpoint these two lock corrections in the case of an unusual shape such as the Savonius rotor. Pope and Barlow [24] suggest that the total correction of tunnel congestion is given by the equation:

$$\xi = \frac{1}{4}\frac{\text{FRONT AREA OF THE MODEL}}{\text{CROSS SECTION AREA OF THE TEST SECTION}}\,. \tag{29}$$

The surface area of the turbine with the stand and the installed accessories was assumed as the face area of the model. The correction factor was set at $\xi = 0.0125$ for a 1 m high rotor and $\xi = 0.0162$ for a 1.5 m high rotor. Later analytical studies showed that the Savonius rotor experiences lateral forces that are of the same order of magnitude as the drag force and equation (29) is imprecise.

Based on the correction of the tunnel congestion, the air velocity v and the dynamic pressure p were corrected:

$$v_{\text{kor}} = (1+\xi)v, \tag{30}$$

$$p_{\text{kor}} = (1+\xi)p. \tag{31}$$

The Reynolds number per unit length is defined as

$$\text{Re} = \frac{\rho v}{\mu}\,. \tag{32}$$

Reynolds numbers refer to a length of 1 m and are an approximate Reynolds number based on the diameter of the turbine. The reason why the Reynolds number is presented as a value per meter is because there is no universally accepted length scale with which to calculate the Reynolds number for a Savonius rotor.

The measurement data of the Savonius rotor was used to calculate the efficiency in the form of torque coefficient C_M and power factor C_P, and presented speed factor λ:

$$C_M = \frac{Q + Q_f}{\frac{1}{2}\rho v^3 A}\,, \tag{33}$$

$$C_P = \frac{\omega(Q + Q_f)}{\frac{1}{2}\rho v^3 A}\,. \tag{34}$$

The results indicate that the static torque coefficient is positive for all angular positions except for the zero gap configuration. The two-blade Savonius rotor exhibits a large variability of the static torque with the change of angular position. On the other hand, the Savonius rotor in the configuration with three blades shows a significantly lower value of the static torque coefficient than the configuration with two blades.

The test results showed that the two-bladed Savonius rotor is insufficient as a starting system for other VAWT wind turbines (Darrieus), because the minimum starting torque is too low in many cases. This problem was solved by using two sets of Savonius rotors, the first of which is rotated by 90° with respect to the second (Fig. 23).

In the two-blade configuration, the Reynolds number has been shown to have an effect on the static torque coefficients as evidenced by shifts in the C_Q torque curves due to delayed separation around the rotor blades with increased Reynolds number. The power factors for all configurations (two blades) peaked at a speed differential of about 0.9 except for the non-slotted configuration where the power factor peaked at a speed differential of about 0.8. The peak power factor for the twin-blade rotor configuration ranges from 0.22 to 0.26 (Fig. 24). The maximum torque ratio occurs at a lower speed ratio, typically around 0.4 for all two-blade configurations, although there is a noticeable increase in power and torque ratio as the Reynolds number increases.

The test data shows the best aerodynamic performance for a gap width of $s/d = 0.1{-}0.15$. The use of both a larger and a smaller gap causes

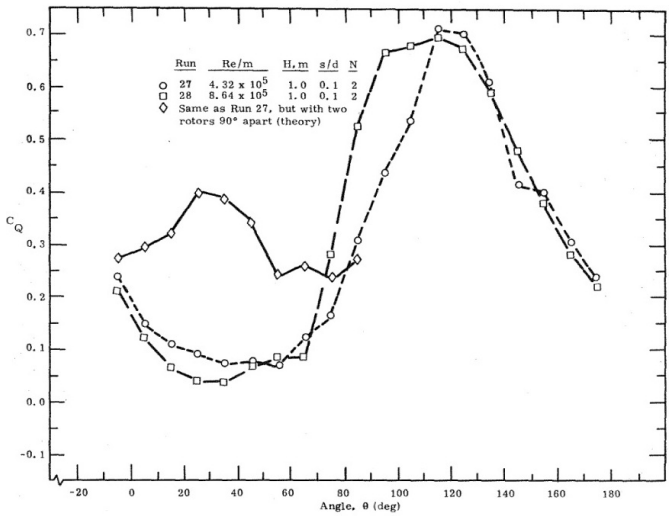

Figure 23: Static coefficient of torque versus angular position for a two-blade Savonius rotor with a slot width ratio of 0.10 for both Re/m values (circle and square) together with the torque curve for a typical hypothetical double-rotated Savonius rotor (rhombus) [24].

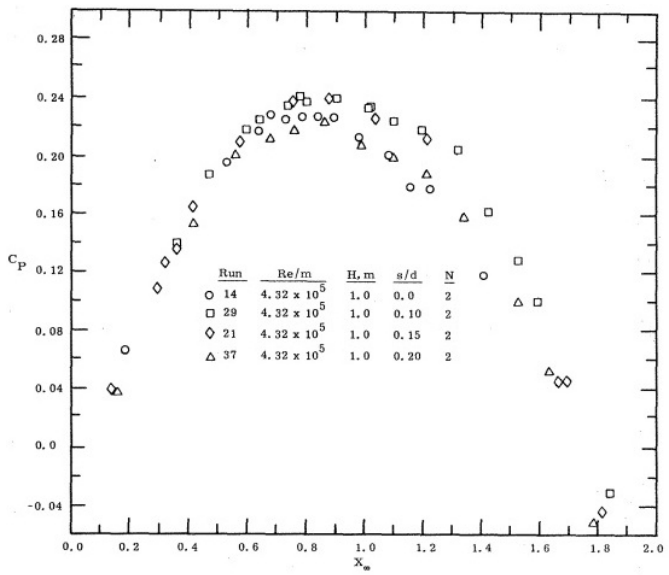

Figure 24: Power factors for 1-metre, two-bladed Savonius rotors with different slot width ratios at Re/m $4.32 \cdot 10^5$ [24].

a decrease in efficiency. The difference in performance is most noticeable with higher gear ratios. A similar trend was achieved for test data with a high Reynolds number. The data clearly indicates that the optimal gap width s/d should be in the range of 0.1 to 0.15 (Fig. 25).

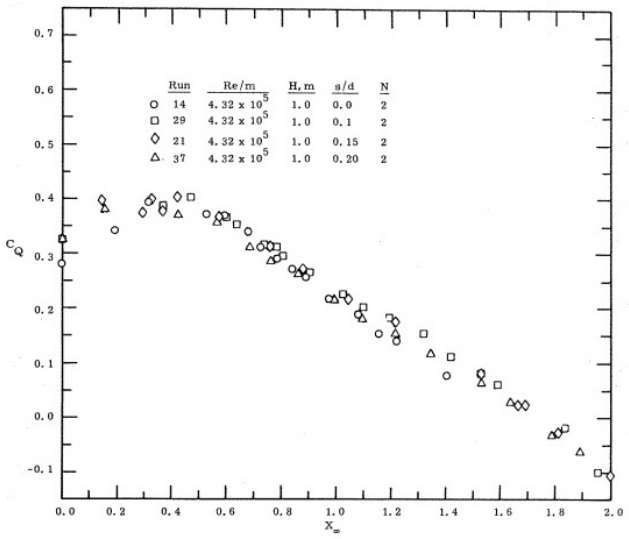

Figure 25: Torque for 1-metre, two-bladed Savonius rotors with different slot width ratios at Re/m $4.32 \cdot 10^5$ [24].

In configurations with three blades, no angular position was observed where the static torque coefficient would be negative. The three-blade configurations showed less variability in the static torque coefficient than the two-blade configurations. The average torque coefficient for one cycle was typically in the range of 0.3 to 0.4 for the three-blade configuration and was analogous to the coefficient for the two-blade configuration. As with the two-blade configuration, the angular position at which the stall occurs was a function of the Reynolds number.

Analysis of the power factor and torque versus turbine speed ratio curves for the three-blade configuration for two Reynolds numbers showed a slight improvement in efficiency with increasing Re. This is not true for all data, and the exact reason for these anomalies where data with a lower Reynolds number has better performance is not known.

From an efficiency point of view, the two-blade configuration is superior in many respects. The maximum power factor in the two-blade configuration is approximately 1.5 times that of the three-blade configura-

tion (Fig. 26). The speed factor at which C_p reaches its maximum value is greater when using a two-blade rotor. The performance advantage of the three-blade configuration over the two-blade configuration is the higher minimum static torque value (Fig. 27), however, this advantage can be eliminated by combining two sets of two-blade rotors into a two-level rotor staggered by 90° from each other.

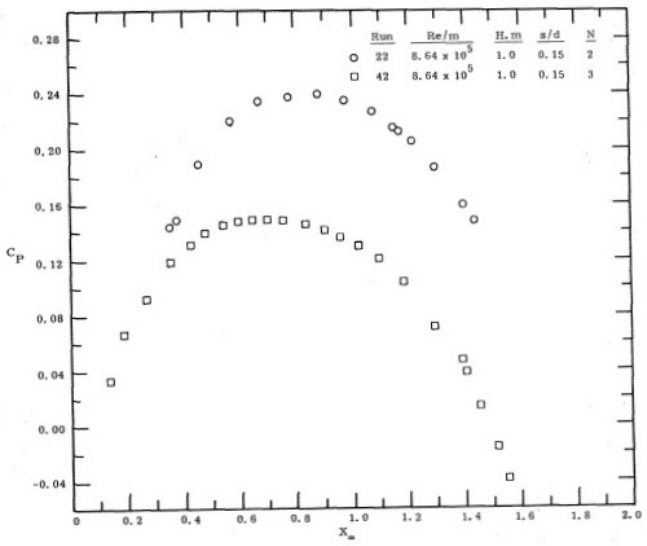

Figure 26: Comparison of the power factors of two- and three-blade Savonius rotors with a slot width ratio 0.15 at Re/m being $8.64 \cdot 10^5$ [24].

The effect of rotor height was tested for the two-blade configuration at $s/d = 0.15$. The fact that the power and torque factors increase slightly with increasing blade height indicates that the endplates provide a reduction in terminal losses. Data for turbines 1.5 m high were comparable to turbines 1 m high (Figs. 28, 29).

Dependencies of the gap width smaller than $s/d = 0.2$ reach approximately the same maximum power and show better parameters than the curve $s/d = 0.2$. At low rotational speeds, the $s/d = 0$ curve seems to be the most favorable, but it shows worse performance at high rotational speeds. Zero gap width exhibits maximum torque, but worse at higher rotational speeds. The configuration with the largest gap width shows the worst performance at low and medium speeds. The general conclusion to be drawn from the data is that the gap is desirable, but should not be large

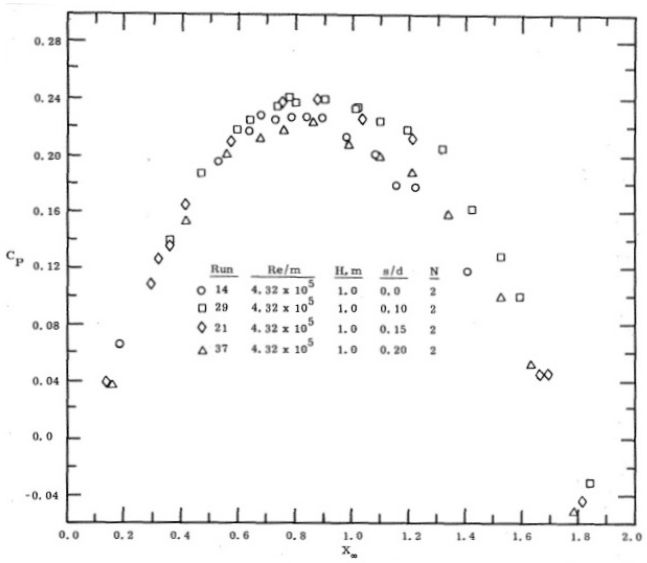

Figure 27: Power coefficients for 1-meter twin-blade Savonius rotors with different gap width ratios at Re/m $4.32 \cdot 10^5$ [24].

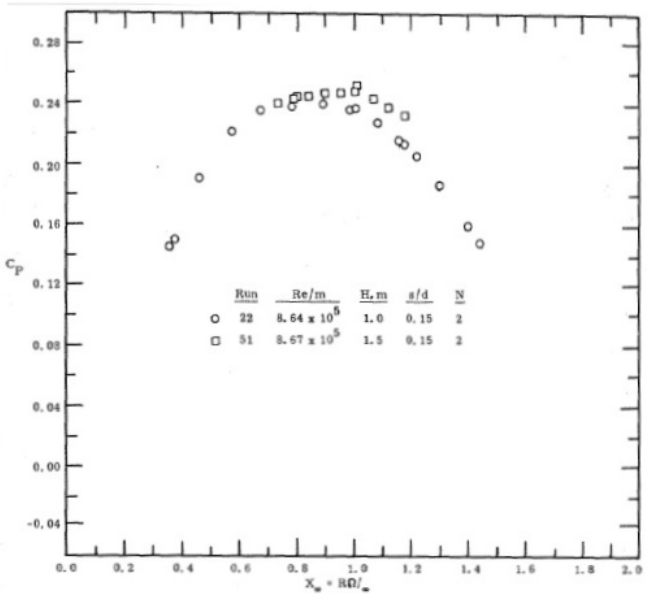

Figure 28: Comparison of power factors for a two-blade configuration with a slot width ratio of 0.15 at Re/m being $8.6 \cdot 10^5$ for two rotor's heights [24].

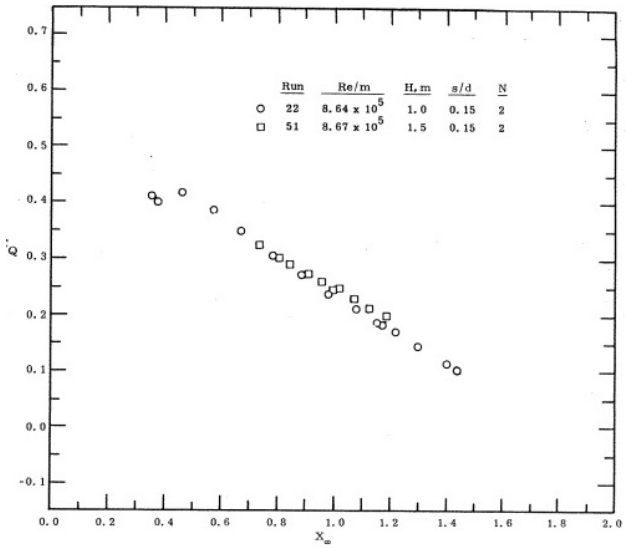

Figure 29: Comparison of torque for a two-blade configuration with slot width ratio 0.15 at Re/m being $8.6 \cdot 10^5$ for two rotor's heights [24].

enough to cause a reduction in the sweep area of the rotor and the radius of rotation.

Summarizing the researches of various configurations of the Savonius rotor, it was found that:

- the static torque coefficient is much more variable with angular position in a two-blade configuration than in a three-blade configuration;
- two-blade configurations have better aerodynamic performance than three-blade configurations, with the exception of starting torque;
- increasing the Reynolds number improves overall aerodynamic performance;
- aerodynamic efficiency slightly increases with increasing height to diameter ratio;
- dimensionless slot width $s/d = 0.1{-}0.15$ for optimal performance;
- for a fixed rotor blade size, the recommended slot width is $s/d = 0.1{-}0.15$;
- the optimal configuration is two sets of two-blade rotors, rotated relative to each other by 90°, each rotor should have a gap of $s/d = 0.1{-}0.15$.

4.3.1 Improving the performance of the Savonius rotor by using quarter blades

The solution of using quarter blades and comparing their efficiency with the conventional model were presented in their studies by Indian scientists [25]. The research was based on CFD (computational fluid dynamics) numerical simulation using the Ansys CFX environment. The validation study was performed on a conventional configuration (Fig. 30), comparing numerical simulation results with [26–50] experimental results for seven different inlet velocities to provide a numerical platform for comparative testing. The way to conduct the comparative study was to set a baseline for comparison and keep other parameters unchanged. The rotor geometry remained the same except for the addition of quarter blades (Fig. 31) so that the maximum dimensions of the rotor remained the same so that the aspect ratio and swept area remained constant for both configurations. The blade overlap ratio and spacing were kept constant.

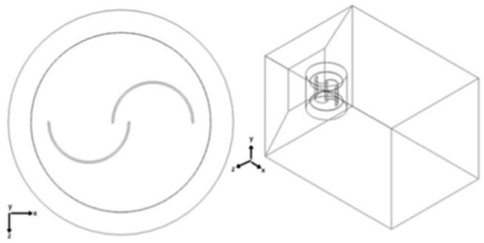

Figure 30: Conventional configuration [25].

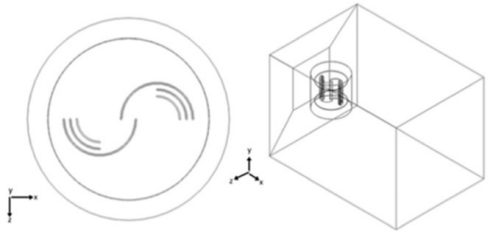

Figure 31: New configuration with quarter blades [25].

A Savonius rotor is a hydrokinetic turbine that uses the kinetic energy of the fluid to generate force on the blade walls. The torque generated on the advancing blade is greater than that on the return blade, providing a net

positive torque. The output torque and C_P of the new and conventional rotor were estimated using a numerical analysis method, with the settings unchanged (Fig. 32).

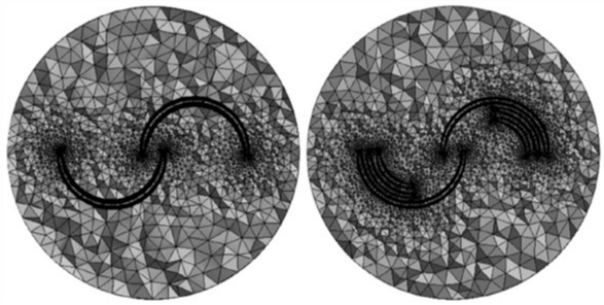

Figure 32: Cross-section view of the mesh generated for the conventional and new configuration [25].

Significant improvements were obtained in efficiency from 8.89% to 13.6%. Under the action of the rotation of the rotor, the fluid surrounding it also begins to rotate. Coverage of the return blade has occurred, but to a limited extent, since the incoming fluid is directed tangentially to the rotational motion of the fluid, but impedes the fluid from impinging on the moving rotor at certain angles. The rotor was placed near the inlet leading to a rapid deflection of the incoming fluid to the periphery of the spinning domain, partially blocking the swirling fluid path (Fig. 33).

The results show a similar trend in torque and power factor for both configurations. The maximum C_P value reached 0.2081 and 0.2266 for an inlet velocity of 8.23 m/s for the conventional and new configurations, respectively, showing an improvement of 8.89%. The maximum improvement in performance was noted for the case of an inlet velocity of 9.21 m/s with an increase in the C_P value of 13.69%. The average rotor torque was evaluated at each time step for all speed reference cases. The distribution of forces on the rotor in the new configuration is shown in Fig. 34.

Each time step corresponds to two degrees of rotation. There was an improvement in the torque performance of the new configuration over the conventional one (Fig. 35). Increasing the exposed area on the pushing side leads to an increase in the effective use of the available kinetic energy from the incoming fluid, also contributing to the increase in positive torque. In order to obtain better accuracy, the torque values generated during the second rotation of the rotor were taken into account for comparison.

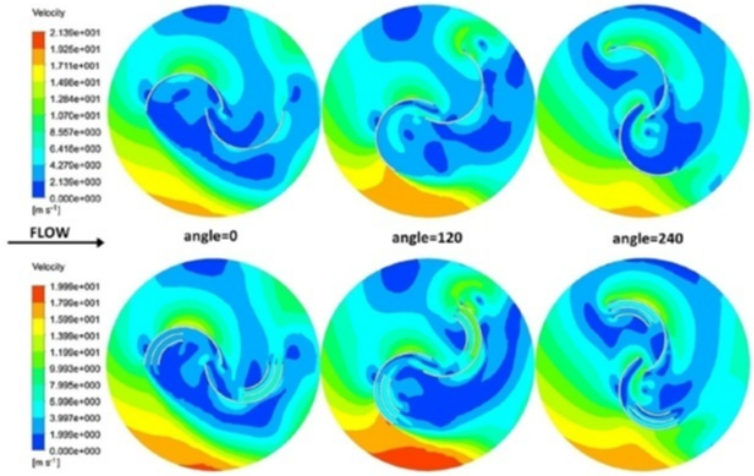

Figure 33: Speed distribution for conventional configuration (above) and new configuration (below) for $V = 8.23$ m/s [25].

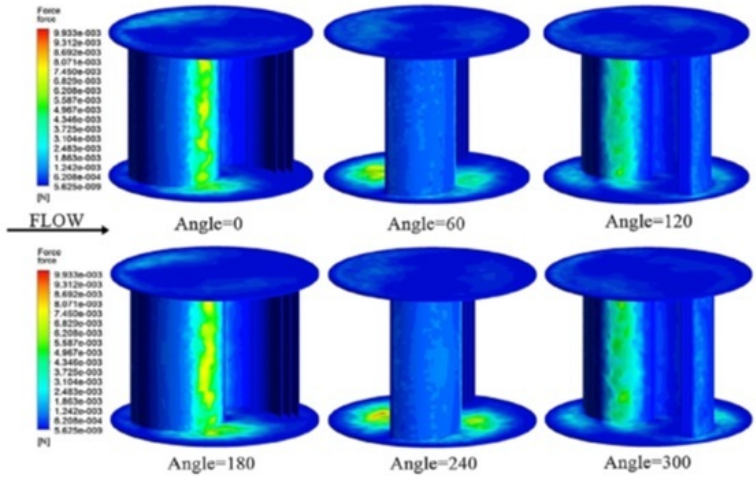

Figure 34: Distribution of forces on the rotor in the new configuration [25].

The numerical validation study was consistent with the experimental data of Saha [26]. In a comparative study, the new configuration was observed to have better performance than the conventional configuration, reaching a maximum C_P value of 0.2266 at $v = 8.23$ m/s with an improvement of 8.89% (Fig. 36).

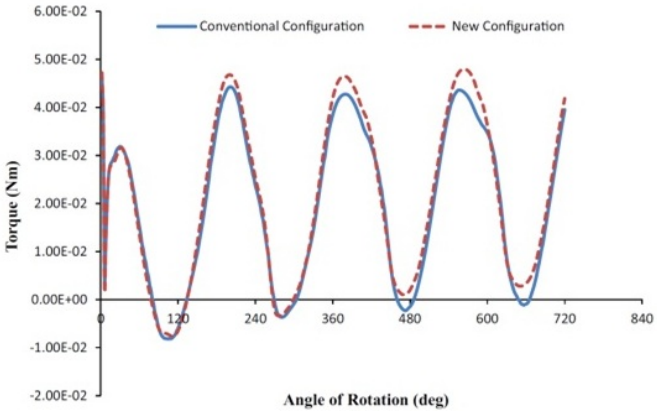

Figure 35: Dependence of the rotor torque on the angle of rotation [25].

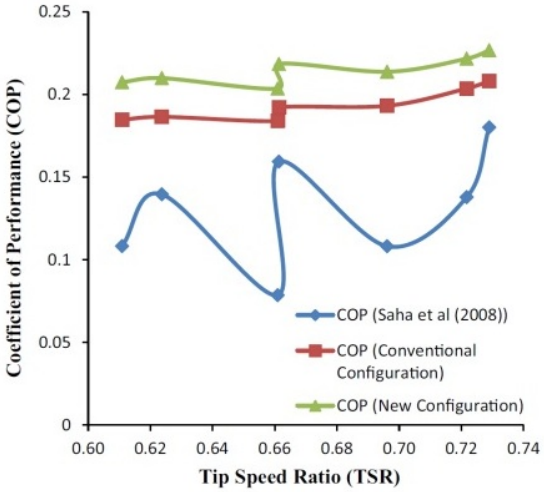

Figure 36: Dependence of the power factor as a function of the speed factor [25].

The tests were carried out keeping the shape factor, external dimensions and flow parameters the same for both configurations in each case. An additional set of quarter blades captures some of the unused kinetic energy of the incoming fluid stream, resulting in in-creased aerodynamic efficiency. The study confirms that the improvement in the performance of the Savonius rotor can be achieved without increasing the spatial parameters and without making complex structural changes to the rotor while maintaining a simple structure.

4.3.2 Optimization of a Savonius turbine with an obstacle shielding the returning rotor blade

The main advantages of the Savonius turbine are simplicity, compactness and strength of the structure as well as low cost, therefore modifications introducing high complexity should not be used. Taking into account the results of previous studies [26,51], some simple guide or deflector plates lead to improved performance at the lowest possible cost and complexity. The influence of the obstacle partially shielding the returning blade of the two- and three-blade Savonius turbines was investigated numerically (Fig. 37). The addition of a shielding obstacle should reduce the negative torque and consequently increase the total torque of the turbine. The position and angle of the shielding obstacle were optimized by a suitable mathematical procedure.

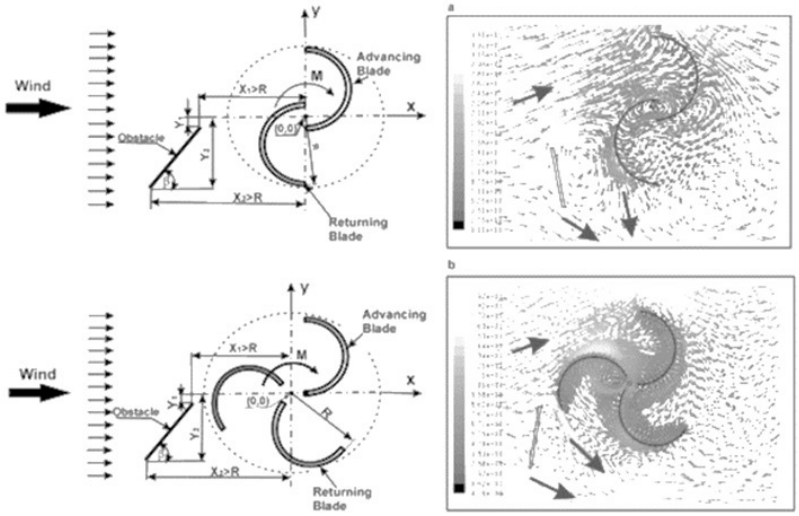

Figure 37: Schematic description and main parameters characterizing the Savonius rotor in configuration with two or three blades, together with a comparison of instantaneous flow structures [52].

By installing an obstacle, the self-starting ability of the turbines was improved. Whereas the conventional two-blade Savonius turbine exhibits negative values for static torque within a certain range, the use of a shielding obstacle resulted in positive static torque at any angle for both designs (Fig. 38). The optimization led to an increase in the output power factor by 27.3%. An increase in the value was observed for the torque factor with

higher values of λ. Taking into account the output power factor obtained and the cost and complexity of the rotor, the two-blade configuration is clearly more efficient than the three-blade turbine. The optimal configuration has peaked the output power factor $C_P = 0.258$ at $\lambda = 0.8$.

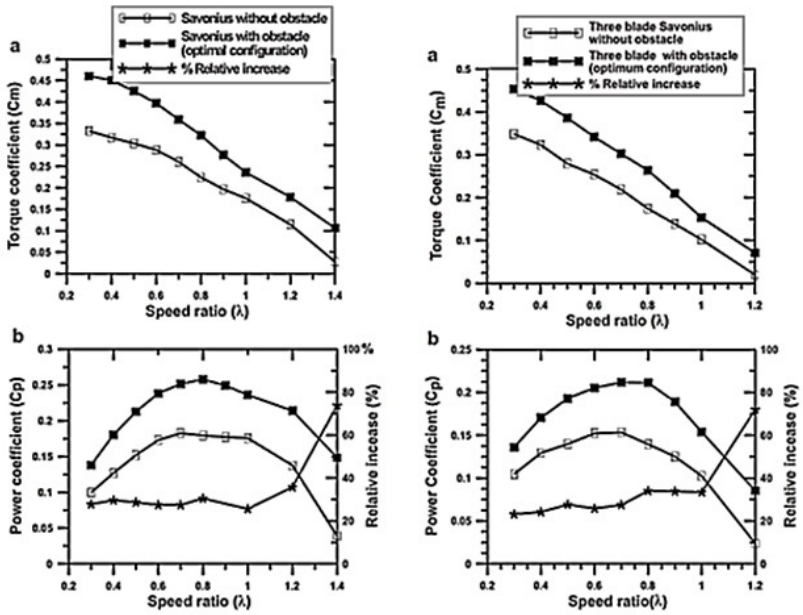

Figure 38: Performance comparison of the conventional configuration without shielding obstacle (white squares), with shielding obstacle (black squares) and relative increments (asterisks) [52].

Using an obstacle shielding the returning blade, an increase in the power and torque coefficients was shown. The optimized configuration is slightly more complex, more expensive and heavier, but guarantees a significant improvement in the aerodynamic parameters of the Savonius turbine with little effort.

5 Conclusions

Summarizing the information presented above, it should be stated that the selection of a wind turbine with a vertical axis of rotation used to generate mechanical and electric energy should be made by analyzing the basic parameters depending on the given structure. The most frequently

considered are the cost of installation and service, applicability, durability and efficiency. However, these systems have both obvious disadvantages and advantages that determine the scope of their use. Referring to the imperfections of these devices, the following should be mentioned first of all: low efficiency, susceptibility to turbulence, torque variability depending on the angular position during rotation, power control limitations at high wind speeds, low-speed units require low-speed generators or gearboxes, which additionally reduces low efficiency, the need to use bearings for the upper part of the rotor due to deviations from the axis of rotation in the absence of it.

However, it should be noted that many more advantages are identified, which include: simple and cheap construction, noiseless operation and its performance regardless of the wind direction (no need to use systems for positioning the turbine perpendicular to the wind), mobility due to easy installation and de-installation, the possibility of installation in the infrastructure s, etc., high aesthetics making it fit into the urban infrastructure, resistance to un-favorable of the urban agglomeration, e.g. on the facades and roofs of buildings, street lamps, lamppost weather conditions such as high-speed winds, atmospheric precipitation, low temperatures, low power losses in basic and movable connections, the generator on the shaft does not require bearing connections.

The conducted analysis indicates that the essence of the use of this type of structure is basically the individual preferences of potential users who belong to the group of the so-called low-enthalpy distributed energy.

Received 19 July 2023

References

[1] Flaga A.: *Wind Engineering: Fundamentals and Applications;* Arkady, Warszawa 2008 (in Polish).

[2] *Atmospheric Structure Available.* https://www.thephysicalenvironment.com/Book/atmosphere/atmospheric_structure.html (accessed 14 Nov. 2022).

[3] Shepherd W., Zhang L.: *Electricity Generation Using Wind Power* (2nd Edn.), World Scientific, New Jersey 2017.

[4] *What Is Global Atmospheric Circulation Available.* https://www.internetgeography.net/topics/what-is-global-atmospheric-circulation/ (accessed 14 Nov. 2022).

[5] Wolańczyk F.: *Wind Power Plants* (2nd Edn.). Wydawnictwo i Handel Książkami KaBe, Krosno 2014 (in Polish).

[6] Maroński R.: *Wind Power Plants.* Wyd. PW, Warszawa 2016 (in Polish).

[7] Jagodziński W.: *Wind Engines.* PWT, Warszawa 1959 (in Polish).

[8] Chauvin A., Benghrib D.: *Drag and lift coefficients evolution of a Savonius rotor.* Exp. Fluids **8**(1989), 118–120. doi: 10.1007/BF00203076

[9] Paraschivoiu I.: *Wind Turbine Design: With Emphasis on Darrieus Concept.* Presses Internat. Polytechnique, Montreal 2009.

[10] Boas M. *Hero's Pneumatica: A study of its transmission and influence.* Isis **40**(1949), 1, 38–48. doi: 10.1086/348993

[11] Cullen C.: *Science and Civilisation in China. Vol. 5: Chemistry and Chemical Technology. Part 2: Spagyrical Discovery and Invention: Magisteries of Gold and Immortality.* China Q. **65**(1976), 143–144. doi: 10.1017/S0305741000031908

[12] Vowles H.P.: *An inquiry into origins of the windmill.* Trans. Newcomen Soc. **11**(1930), 1–14. doi: 10.1179/tns.1930.001

[13] White L.: *Medieval Technology and Social Change.* Oxford Univ. Press, London 1980.

[14] Drachman R.J.: *Extension of the variational method for Hard-Sphere Bosons.* Phys. Rev. **121**(1961), 643–647. doi: 10.1103/PhysRev.121.643

[15] Greenwood J.G., Woodcroft B.: *The Pneumatics of Hero of Alexandria, From the Original Greek.* History of science library. London, Taylor, Walton and Maberly, 1851.

[16] Hero of Alexandria, Schmidt W.: *Herons Von Alexandria Druckwerke Und Automatentheater = Pneumatica et Automata.* Legare Street Press, 2022.

[17] Bellew H.W.: *From the Indus to the Tigris.* Creative Media Partners, LLC 2018.

[18] Hedin S.A.: *Overland to India:* Vol. 2. Creative Media Partners, LLC 2018.

[19] Wulff H.E.: *The Traditional Crafts of Persia: Their Development, Technology, and Influence on Eastern and Western Civilizations.* MIT. Press, 1966.

[20] Spera D.A.: *Wind Turbine Technology: Fundamental Concepts of Wind Turbine Engineering.* ASME Press, 2009.

[21] Lyatkher V.M.: *Wind Power: Turbine Design, Selection, and Optimization.* Wiley, 2013.

[22] Wolniewicz K., Kuczyński W., Zagubień A.: *Method for wind turbine selection basing on in-field measurements.* J. Mech. Energy Eng. **3**(2019), 77–84. doi: 10.30464/jmee.2019.3.1.77

[23] Sheldahl R.E., Blackwell B.F., Feltz L.V.: *Wind tunnel performance data for two- and three-bucket Savonius rotors.* J. Energy **2**(1978), 160–164. doi: 10.2514/3.47966

[24] Pope A., Barlow J.R., Rae W.H.: *Low-Speed Wind Tunnel Testing.* Wiley India Pvt, 2010.

[25] Sharma S., Sharma R.K.: *Performance improvement of Savonius rotor using multiple quarter blades – a CFD investigation.* Energy Convers. Manage. **127**(2016), 43–54. doi: 10.1016/j.enconman.2016.08.087

[26] Saha U.K., Rajkumar M.J.: *On the performance analysis of Savonius rotor with twisted blades.* Renew. Energy **31**(2006), 1776–1788. doi: 10.1016/j.renene.2005.08.030

[27] Akwa J.V., Alves da Silva Júnior G., Petry A.P.: *Discussion on the verification of the overlap ratio influence on performance coefficients of a Savonius wind rotor using computational fluid dynamics*. Renew. Energy **38**(2012), 141–149. doi: 10.1016/j.renene.2011.07.013

[28] Akwa J.V., Vielmo H.A., Petry A.P.: *A review on the performance of Savonius wind turbines*. Renew. Sustain. Energy Rev. **16**(2012), 3054–3064. doi: 10.1016/j.rser.2012.02.056

[29] Alexander A.J., Holownia B.P.: *Wind tunnel tests on a Savonius rotor*. J. Wind Eng. Ind. Aerodyn. **3**(1978), 343–351. doi: 10.1016/0167-6105(78)90037-5

[30] Aslam Bhutta M.M., Hayat N., Farooq A.U., Ali Z., Jamil Sh.R., Hussain Z.: *Vertical axis wind turbine – a review of various configurations and design techniques*. Renew. Sustain. Energy Rev. **16**(2012), 1926–1939. doi: 10.1016/j.rser.2011.12.004

[31] Boczar T.: *Use of Wind Energy* (2nd Edn.). Wydawn. PAK, Warszawa 2010 (in Polish).

[32] Fujisawa N.: *On the torque mechanism of Savonius rotors*. J. Wind Eng. Ind. Aerodyn. **40**(1992), 277–292. doi: 10.1016/0167-6105(92)90380-S

[33] Jeon K.S., Jeong J.I., Pan J.K., Ryu K.W.: *Effects of end plates with various shapes and sizes on helical Savonius wind turbines*. Renew. Energy **79**(2015), 167–176. doi: 10.1016/j.renene.2014.11.035

[34] Kumbernuss J., Chen J., Yang H.X., Lu L.: *Investigation into the relationship of the overlap ratio and shift angle of double stage three bladed vertical axis wind turbine (VAWT)*. J. Wind Eng. Ind. Aerodyn. **107−108**(2012), 57–75. doi: 10.1016/j.jweia.2012.03.021

[35] Manwell J.F., MacGowan J.G., McGowan J.G., Rogers A.L.: *Wind Energy Explained: Theory, Design and Application*. Wiley, 2009.

[36] Saha U.K., Thotla S., Maity D.: *Optimum design configuration of Savonius rotor through wind tunnel experiments*. J. Wind Eng. Ind. Aerodyn. **96**(2008), 1359–1375. doi: 10.1016/j.jweia.2008.03.005

[37] Posa A., Parker C.M., Leftwich M.C., Balaras E.: *Wake structure of a single vertical axis wind turbine*. Int. J. Heat Fluid Flow **61**(2016), 75–84. doi: 10.1016/j.ijheatfluidflow.2016.02.002

[38] Shahizare B., Nik-Ghazali N., Chong W.T., Tabatabaeikia S., Izadyar N., Esmaeilzadeh A.: *Novel investigation of the different omni-direction-guide-vane angles effects on the urban vertical axis wind turbine output power via three-dimensional numerical simulation*. Energy Convers. Manage. **117**(2016), 206–217. doi: 10.1016/j.enconman.2016.03.034

[39] Yin C., Zhang Z., Wang Z., Guo H.: *Numerical simulation and experimental validation of ultrasonic De-Icing system for wind turbine blade*. Appl. Acoust. **114**(2016), 19–26. doi: 10.1016/j.apacoust.2016.07.004

[40] Wekesa D.W., Wang C., Wei Y., Zhu W.: *Experimental and numerical study of turbulence effect on aerodynamic performance of a small-scale vertical axis wind turbine*. J. Wind Eng. Ind. Aerodyn. **157**(2016), 1–14. doi: 10.1016/j.jweia.2016.07.018

[41] Nezamolmolki D., Shooshtari A.: *Investigation of nonlinear dynamic behavior of lattice structure wind turbines*. Renew. Energy **97**(2016), 33–46. doi: 10.1016/j.renene.2016.05.070

[42] Wang L., Kolios A., Nishino T., Delafin P.L., Bird T.: *Structural optimisation of vertical-axis wind turbine composite blades based on finite element analysis and genetic algorithm*. Compos. Struct. **153**(2016), 123–138. doi: 10.1016/j.compstruct.2016.06.003

[43] Akbar M.A., Mustafa V.: *A new approach for optimization of vertical axis wind turbines*. J. Wind Eng. Ind. Aerodyn. **153**(2016), 34–45. doi: 10.1016/j.jweia.2016.03.006

[44] Giahi M.H., Dehkordi A.J.: I*nvestigating the influence of dimensional scaling on aerodynamic characteristics of wind turbine using CFD simulation*. Renew. Energy **97**(2016), 162–168. doi: 10.1016/j.renene.2016.05.059

[45] Li Q., Murata J., Endo M., Maeda T., Kamada Y.: *Experimental and numerical investigation of the effect of turbulent inflow on a horizontal axis wind turbine (part II: Wake characteristics)*. Energy **113**(2016), 1304–1315. doi: 10.1016/j.energy.2016.08.018

[46] Campobasso M.S., Drofelnik J., Gigante F.: *Comparative assessment of the harmonic balance Navier–Stokes technology for horizontal and vertical axis wind turbine aerodynamics*. Comput. Fluids **136**(2016), 354–370. doi: 10.1016/j.compfluid.2016.06.023

[47] Chong W.T., Gwani M., Shamshirband S., Muzammil W.K., Tan C.J., Fazlizan A., Poh S.C., Petković D., Wong K.H.: *Application of adaptive neuro-fuzzy methodology for performance investigation of a power-augmented vertical axis wind turbine*. Energy **102**(2016), 630–636. doi: 10.1016/j.energy.2016.02.082

[48] Zuo W., Wang X., Kang S.: *Numerical simulations on the wake effect of H-type vertical axis wind turbines*. Energy **106**(2016), 691–700. doi: 10.1016/j.energy.2016.02.127

[49] Jia X., Jin C., Buzza M., Wang W., Lee J.: *Wind turbine performance degradation assessment based on a novel similarity metric for machine performance curves*. Renew. Energy **99**(2016), 1191–1201. doi: 10.1016/j.renene.2016.08.018

[50] Wang Y, Sun X., Dong X., Zhu B., Huang D., Zheng Z.: *Numerical investigation on aerodynamic performance of a novel vertical axis wind turbine with adaptive blades*. Energy Convers. Manage. **108**(2016), 275–286. doi: 10.1016/j.enconman.2015.11.003

[51] Menet J.L.: *A double-step Savonius rotor for local production of electricity: A design study*. Renew. Energy **29**(2004), 1843–1862. doi: 10.1016/j.renene.2004.02.011

[52] Mohamed M.H., Janiga G., Pap E., Thévenin D.: *Optimization of Savonius turbines using an obstacle shielding the returning blade*. Renew. Energy **35**(2010), 2618–2626. doi: 10.1016/j.renene.2010.04.007